ADAPTIVE FILTERING OF RFI IN WIDEBAND SAR SIGNALS

Charles TC Le, Scott Hensley, and Elaine Chapin

Jet Propulsion Laboratory, California Institute of Technology
4800 Oak Grove Drive, Pasadena, CA 91109

Abstract

The least-mean-square (LMS) adaptive filter is applied to suppress narrow-band radio-frequency interference (RFI) in wideband synthetic aperture radar (SAR) signals. Simulation is used to show the working principles of the adaptive filter. The filter performance with respect to the filter parameters (filter length, delay, and step size) is analyzed in terms of the radar performance parameters such as the integrated sidelobe ratio (ISLR) and peak sidelobe ratio (PSLR). Finally, the algorithm is tested with data in different noisy environments, collected in the JPL P-band TopSAR program.

1 Introduction

The problem of removal (or enhancement) of narrow-band interference from wideband signals has long been an active research topic in various disciplines. Examples can be found in the signal processing [1], communications [2], and lately in radar [3, 4] and image processing [5] communities. Adaptive filters [6, 7] have played a vital part in solving this problem. The most popular adaptive filtering technique is the LMS algorithm, which has enjoyed enormous popularity due to its good compromise for the convergence speed, final misadjustment, stability and complexity, that are usually required at the same time. This algorithm utilizes a gradient search technique to determine the filter coefficients which minimize the mean square prediction error [6]. The LMS algorithm requires only 2N operations per iteration for real data (N for complex data) and no explicit determination of the correlation coefficients of the input data [8].

The LMS filter in Fig. 1 can be intuitively described as follows. The delay Δ causes decorrelation between the wideband components (radar signal) of the primary input d and the reference input x. The adaptive filter tries to estimate the narrow-band component

y (RFI signal), and in doing so, effectively forms an equivalent transfer function, which is similar to that of narrow-band filters centered at the frequencies of the narrow-band components of the input signal. The wideband component of the delayed input is rejected, while the phase difference of the narrow-band components is readjusted so that they cancel each other at the summing junction, producing a minimum error signal consisting of mainly the wideband component. Uses of the LMS adaptive filter to detect signals (such as sinusoids, narrow-band and chirp-like signals, ...) in white Gaussian noise have been described in [8].

In this study, we will apply the LMS algorithm to remove narrow-band RFI from wide-band SAR signals. We first describe the point target simulator. Then, the stability and convergence of the filter are analyzed in details in terms of the filter parameters (filter length, delay, and step size) and input characteristics (signal bandwidth, sampling rate, and SNR). It has been shown that the filter output converges more rapidly than the filter weights [8]. Consequently, the evaluation of the filter performance is based on the SAR compressor output with the help of the radar parameters, such as ISLR and PSLR. Finally, we will show cleaned images obtained by applying the adaptive filter to data collected by the JPL P-band TopSAR systems [9].

2 The LMS Algorithm

The LMS adaptive filter is shown in Fig. 1 and consists of an L-weight linear prediction filter in which the coefficients $w_l(k)$ are adaptively updated at the input sampling rate, f_s. We define the L-element input and weight vectors as $\mathbf{d}(n) = [d(n), d(n-1), \ldots, d(n-L+1)]^T$ and $\mathbf{w}(n) = [w_0(n), w_1(n), \ldots, w_{L-1}(n)]^T$, respectively. The superscript T denotes the matrix transpose. In the RFI suppression problem, a reference signal is obtained by delaying the received signal $d(n)$ to give $x(n) = d(n-\Delta)$ for some time delay Δ. The output of the filter is a linear combination of these delayed past input values weighted by the filter weight vector

$$y(n) = \mathbf{w}^T(n) \cdot \mathbf{x}(n) = \mathbf{w}^T(n) \cdot \mathbf{d}(n-\Delta) \tag{1}$$

This gives an estimate of the RFI signal. The prediction error, which is the radar signal of interest, is obtained by subtracting the RFI estimate y from the received signal d

$$e(n) = d(n) - y(n) \tag{2}$$

The value of Δ is chosen to remove the correlation between the wideband components of the input signal $d(n)$ and the (predicted) filter output $y(n)$. The filter weights $\mathbf{w}(n)$ are selected so as to minimize the mean square error (MSE) $E[e^2(n)]$, where E[.] is the expectation operator. The Widrow-Hoff LMS algorithm leads to a recursive relation for updating the weight vector [6, 7]

$$\mathbf{w}(n+1) = \mathbf{w}(n) + \mu \mathbf{x}(n) e^*(n) \tag{3}$$

where μ is the adaptation constant or step-size parameter. This parameter controls the trade-off between convergence speed and final misadjustment [6, 7, 8]. Large value of μ leads to faster convergence at the expense of large final misadjustment. Its value is preselected based on the desired performance characteristics which, in our case, are the radar performance parameters.

3 The Point-Target Simulator

The point-target simulator, used in verifying the algorithm and making parameter selections, is shown in Fig. 2. The radar's parameters are specified in the left-top corner. Noise consists of thermal random noise, discrete sinusoidal tones, and narrow-band modulation signals (AM, FM, ...). They are characterized by their amplitudes, frequency locations, and bandwidths with respect to the radar signal. In the future GeoSAR system (operational in Sept. 1999), a sniffer pulse is also allowed to measure the RFI environment. The combined radar-and-noise signal is fed into an A/D converter using either 8-bit or block-floating-point (BFPQ) quantization scheme. The A/D output is the input to the LMS adaptive filter which gives as its outputs the estimated RFI signal and the cleaned radar signal. Fig. 3 shows the time-domain waveforms and frequency spectra of the components of the total signal. The chirp signal has a bandwidth of 40 MHz and its signal-to-noise ratio (SNR) is 10 dB. The RFI consists of 6 tones and 2 FM signals. The tones are at frequencies ± 3, ± 10, and ± 15 MHz, with amplitudes (interference-to-signal ratio, ISR) 12, 13, and 17 dB, respectively. The FM signals have center frequencies of ± 12 MHz, with bandwidth of 100 kHz (typical for FM radio channels), and ISR of 15 dB. The initial phases of all RFI signals are picked at random.

4 Simulation Results, Performance Analysis, and Real Images

4.1 Simulation Results and the Radar Parameters

Fig. 4 compares the signal waveforms and spectra of the input, output, and ideal signals. As evident from the output spectra, most of RFI energy has been removed and the output waveform is close to the ideal case. Fig. 5 shows the outputs of the pulse compression filter for the unfiltered, filtered, and ideal radar signals. The presence of RFI makes it impossible to detect the target (top graph). The adaptive filter helps in reducing the sidelobe energy and enhance the target visibility (middle graph). The compressor output of the filtered signal compares favorably with the ideal case (bottom graph). In order to evaluate the

algorithm, it is necessary to define some performance parameters. Among the parameters useful for characterizing filter performnace are the ISLR and PSLR. The ISLR is the ratio of the energy in the sidelobe to the energy in the main lobe. And the PSLR is the ratio of the peak value of the sidelobe to the peak value of the main lobe. Let $g(r)$ denotes the output of the compressor filter, the ISLR and PSLR are defined as

$$ISLR = \frac{\int_{SL} |g(r)|^2}{\int_{ML} |g(r)|^2} \tag{4}$$

$$PSLR = \frac{\max_{SL} \{g(r)\}}{\max_{ML} \{g(r)\}} \tag{5}$$

4.2 Performance with Respect to the Filter Parameters

The design parameters for the LMS adaptive filter are the filter length L, the delay Δ and the step size μ. The objective is to study the variation of the performance parameters, ISLR and PSLR, in terms of these design parameters. Since there is no closed form solution relating these two sets of parameters, one simulation technique is to fix all but one parameter at each simulation stage. For example, we first let $L = 512$, $\Delta = 1$, and study the behavior of ISLR and PSLR as functions of the step-size parameter μ. The results are shown in Fig. 6. The top (bottom) horizontal line indicates the limiting values in the case of unfiltered (ideal) signal. The filter performance will be somewhere in between. The simulation is repeated for the other two design parameters L and Δ, and the results are plotted in Figs. 7 and 8. The optimal values for the filter's parameters are $L = 512$, $\mu = 0.1$, and $\Delta = 1$, corresponding to gains of 25 dB and 22 dB for the ISLR and PSLR, respectively (see Fig. 8). These optimal values were used to produce the results in Figs. 4 and 5.

4.3 JPL P-Band TopSAR Images

Using the optimal design parameters given above, we have applied the LMS adaptive filter to a test site in Mount Sonoma, California. The data has been acquired by the JPL P-band (40 MHz) TopSAR instrument [9] in 1995. The average spectra of 100,000 lines are plotted in Fig. 9. The top spectrum clearly shows the presence of RFI which was effectively cleaned as shown on bottom graph. And finally, Fig. 10 displays the RFI-contaminated range-Doppler image (left) and the corresponding cleaned image (right).

5 Conclusion

We have presented an adaptive filtering technique to remove RFI from wideband SAR signals. The filter employs the least-mean-square algorithm to update the filter weights. This weight update scheme requires no matrix solving or the calculations of the correlation coefficients.

The filter design is very simple since there are only three design parameters. Yet, the filter can adapt to the noisy RFI environment. We have also described the simulation procedure to show the filter's working principle and to obtain the optimal values for the design parameters. Finally, we have displayed the RFI-contaminated image and compared it with a much improved image. Our future efforts include fast versions of the adaptive filter and automatic determination of the design parameters.

Acknowledgment: The authors would like to thank Dr. M. Davis of DARPA and Dr. P. Tomlinson of DSA for their support and useful suggestions, and Dr. C. Werner of JPL for thoughtful discussion. This work has been done at the Jet Propulsion Laboratory, California Institute of Technology, under contract with the National Aeronautics and Space Administration.

References

[1] B. Widrow, J. Glover, J. McCool, J. Kaunitz, C. Williams, K. Hearn, J. Zeidler, E. Dong, Jr., and R. Goodin, "Adaptive noise cancelling: principles and applications", *Proc. of the IEEE*, vol. 63, pp. 1692-1716, 1975.

[2] L. Milstein, "Interference rejection techniques in spread spectrum communications", *Proc. of the IEEE*, vol. 76, pp. 657-71, 1988.

[3] M. Braunstein, J. Ralston, and D.Sparrow, "Signal processing approaches to radio frequency interference suppression", in *Algorithms for Synthetic Aperture Radar Imagery*, Dominick A. Giglio, Editor, Proc. SPIE 2230, pp.190-208, 1994.

[4] Session 3: Radio Frequency Interference Rejection, in *Algorithms for Synthetic Aperture Radar Imagery II*, Dominick A. Giglio, Editor, Proc. SPIE 2487, pp. 72-129, 1995.

[5] T. Soni, J.R. Zeidler, and W.H. Ku, "Performance evaluation of 2-D adaptive prediction filters for detection of small objects in image data", *IEEE Trans. Image Processing*, vol. 2, pp. 327-340, 1993.

[6] B. Widrow and S.D. Stearns, "Adaptive Signal Processing", Englewood Cliffs, N.J.: Prentice-Hall, 1984.

[7] S. Haykin, "Adaptive Filter Theory", Englewood Cliffs, N.J.: Prentice-Hall, 1991.

[8] J.R. Zeidler, "Performance analysis of LMS adaptive prediction filters", *Proc. of the IEEE*, vol. 78, pp. 1781-1806, 1990.

[9] H. A. Zebker, S. N. Madsen, J. Martin, K. B. Wheeler, T. Miller, Y. Lou, G. Alberti, S. Vetrella, and A. Cucci, "The TOPSAR interferometric radar topographic mapping instrument", *IEEE Trans. Geosci. Remote Sensing*, vol. 30, no. 5, pp. 933-940, 1992

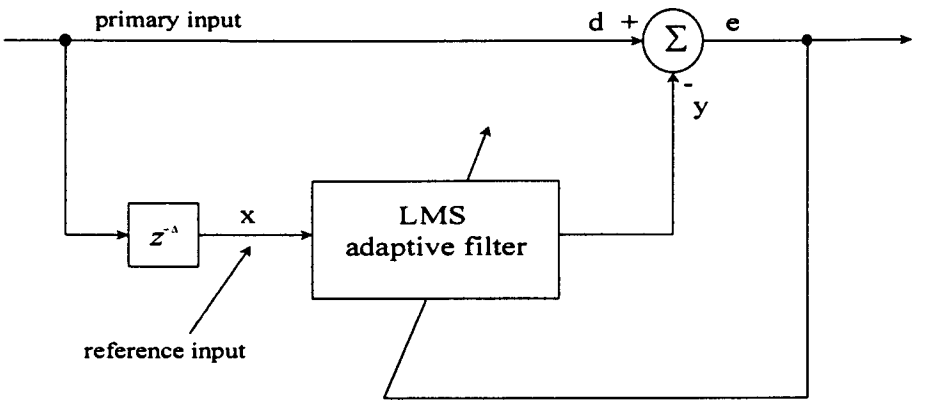

Figure 1: The LMS adaptive filter

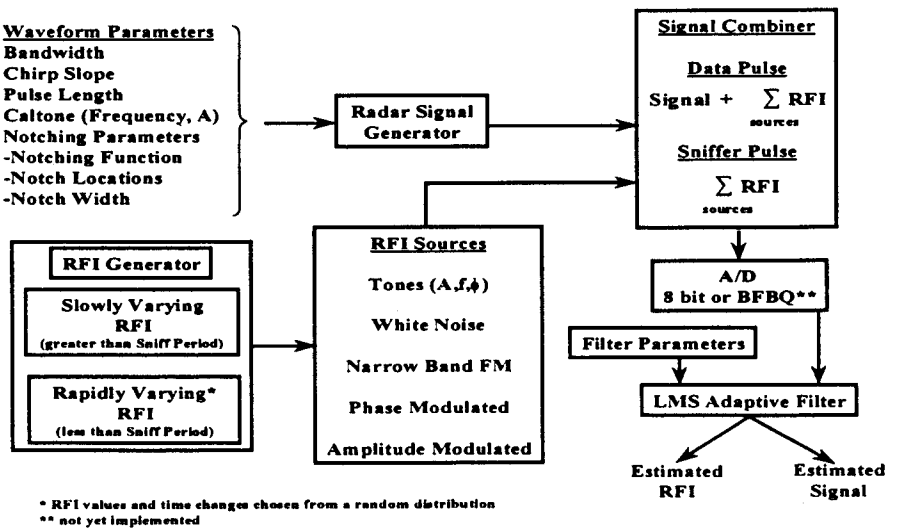

Figure 2: RFI Simulator Block Diagram

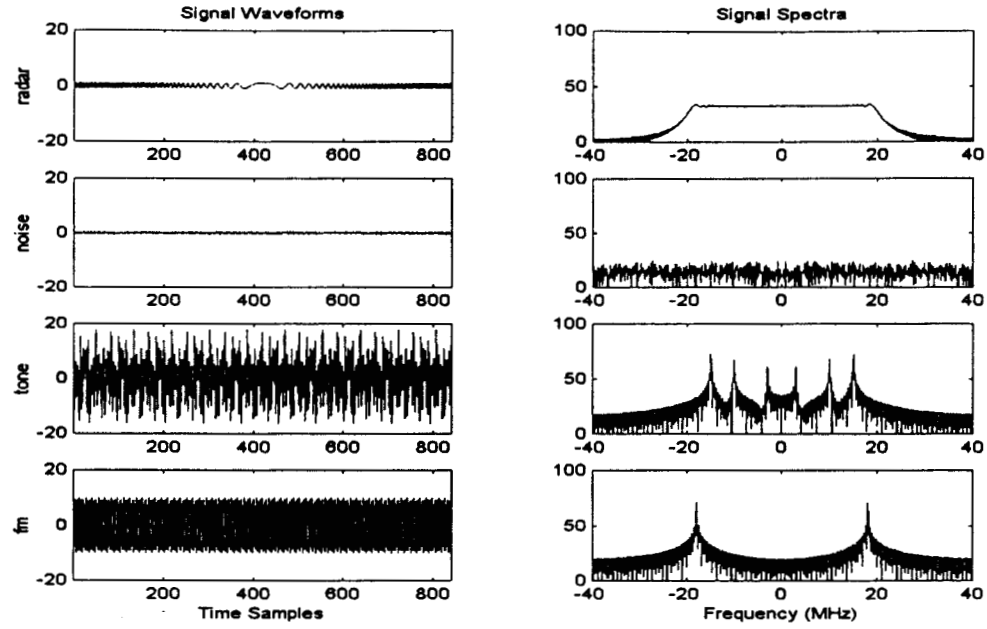

Figure 3: Time-Domain and Frequency-Domain Components of Total Signal

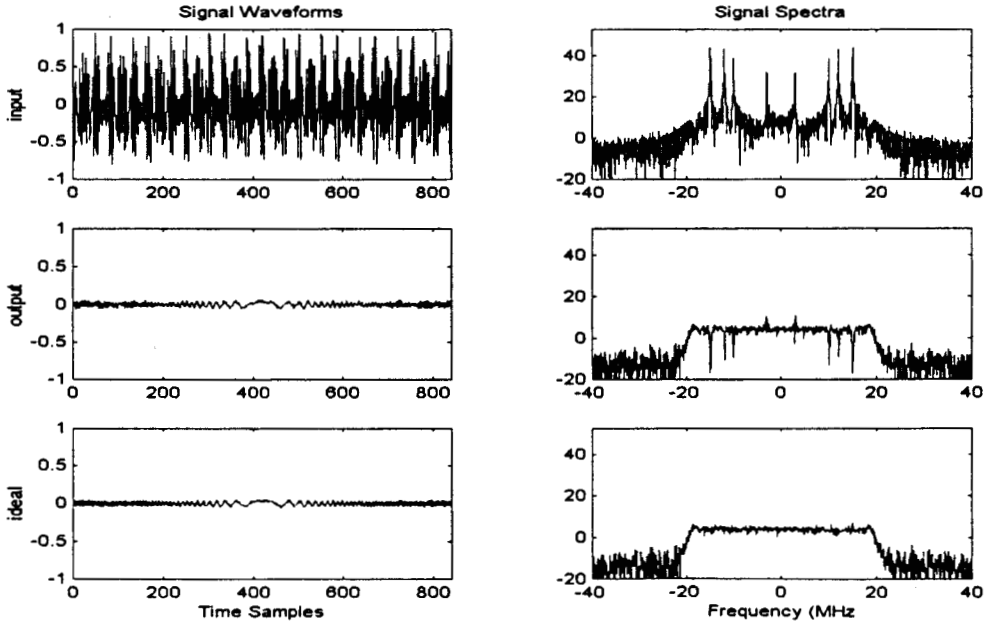

Figure 4: Comparison of Signal Waveforms and Spectra

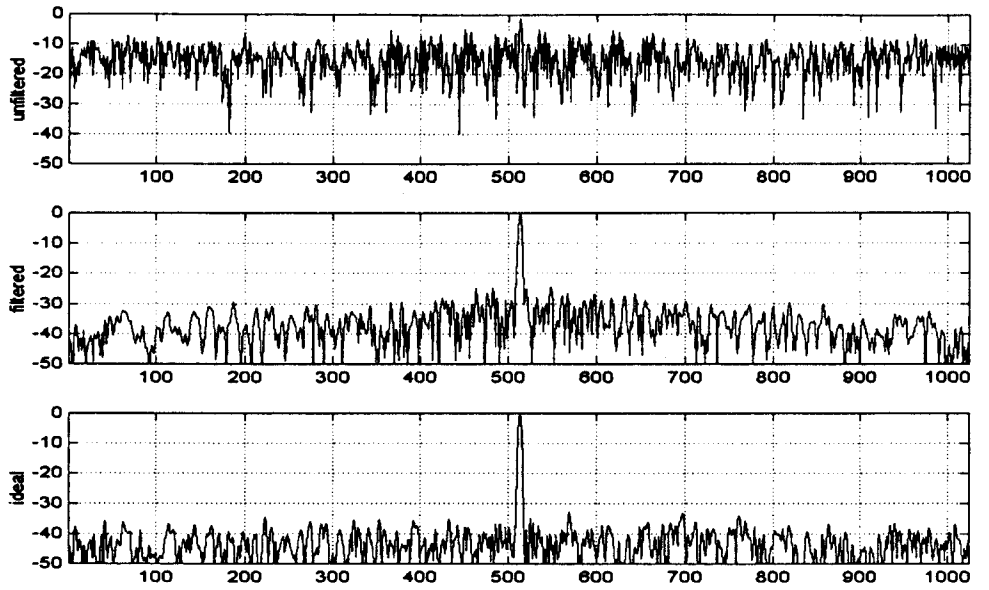

Figure 5: Comparison of Outputs of Pulse Compression Filter

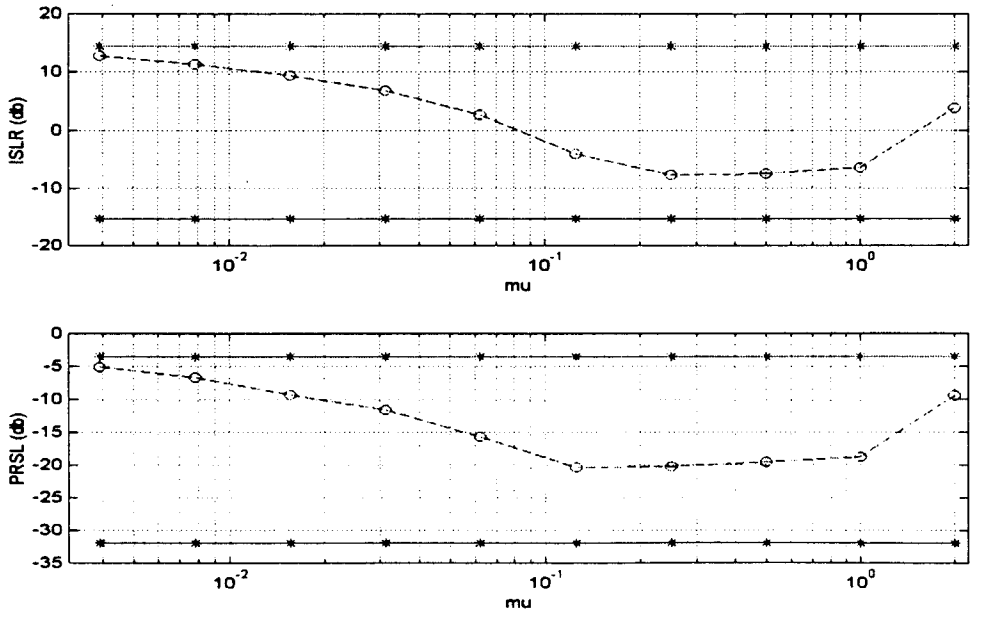

Figure 6: Performance Parameters ISLR and PSLR in terms of the Step-Size Parameter μ

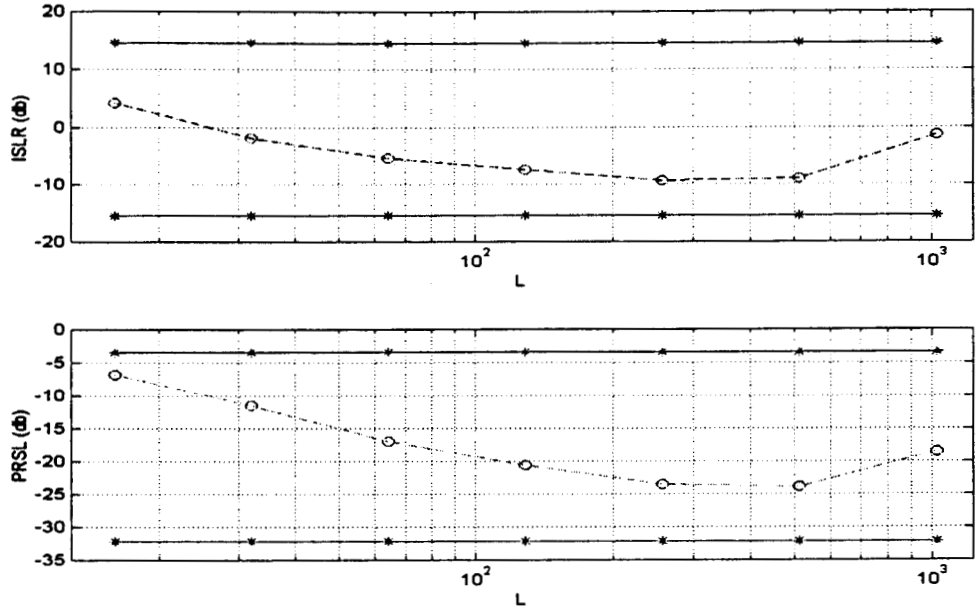

Figure 7: Performance Parameters ISLR and PSLR in terms of the Filter Length L

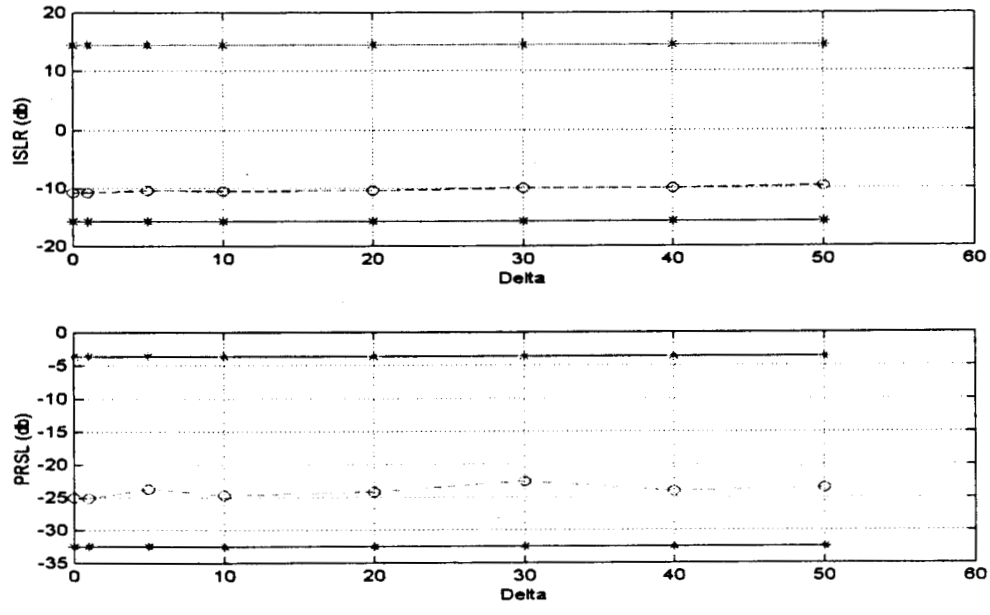

Figure 8: Performance Parameters ISLR and PSLR in terms of the Delay Δ

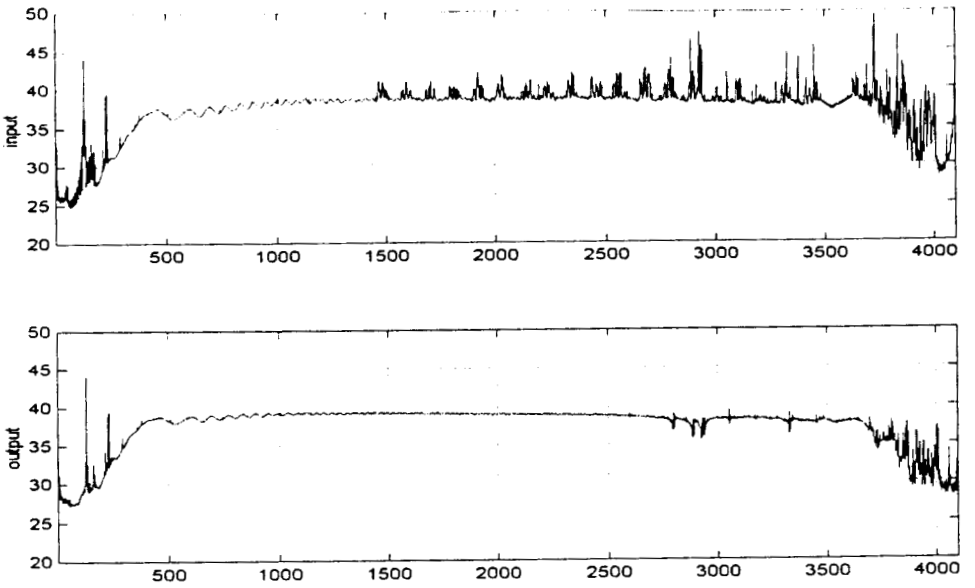

Figure 9: Average Spectrum of 100,000 Pulses (top: unfiltered, bottom: filtered).

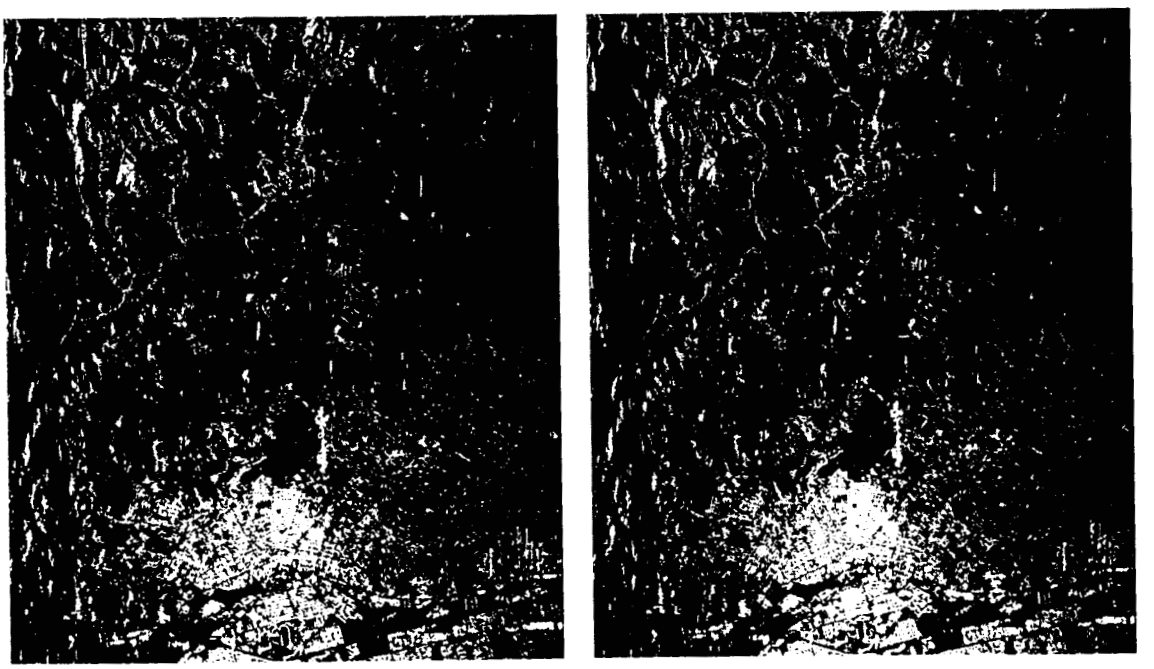

Figure 10: Range-Doppler Images (left: RFI contaminated, right: cleaned).